



Simultaneous description of charge, mass, total kinetic energy, and neutron multiplicity distributions in fission of Th and U isotopes

H. Paşca 

*Joint Institute for Nuclear Research, 141980 Dubna, Russia
and “Babeş-Bolyai” University, Faculty of Physics, 400084 Cluj-Napoca, Romania*

A. V. Andreev, G. G. Adamian , and N. V. Antonenko

Joint Institute for Nuclear Research, 141980 Dubna, Russia



(Received 6 May 2021; revised 28 May 2021; accepted 21 June 2021; published 6 July 2021)

For fissioning isotopes of thorium and uranium, the simultaneous description of the charge, mass, total kinetic energy, and neutron multiplicity distributions of fission fragments is presented within the improved scission-point model. Correlations between all these observables are analyzed. The influence of the transition from symmetric to asymmetric fission mode on the shape of neutron multiplicity distribution is studied.

DOI: [10.1103/PhysRevC.104.014604](https://doi.org/10.1103/PhysRevC.104.014604)

I. INTRODUCTION

The study of nuclear fission process has been an arduous and continuous undertaking for almost nine decades, and still some of the most interesting and striking features are not fully understood. While the experimental data and theoretical predictions are still missing in some regions of the nuclide chart, new data seem to constantly provide new challenges [1]. For example, the role of shell corrections is still not understood to a satisfactory level, especially if one considers the evolution of the mass and charge distributions of fission fragments with the excitation energy of the compound nucleus (CN). In recent experiments [2–12], the asymmetric fission modes have been observed even at high excitation energies, while so far the general understanding is that, with an increase of excitation energy, the symmetric fission mode is the only one preserved. So, the competition between symmetric and asymmetric fission modes with increasing excitation energy is still a matter of study. Another question of interest is represented by the scission configuration itself; it is known from the measured total kinetic energy (TKE) data that the fission fragments are deformed at scission point. This has several consequences on the fission observables: On the one hand, the deformation of the fragments leads to a decrease of the interaction potential and, accordingly, to a decrease of the potential energy of the system; this, in turn, leads to a higher excitation energy and increased attenuation of the shell effects. The combined effect leads to a change of the potential energy surface (PES) and, ultimately, to a change in the shape of the mass and charge distributions. On the other hand, after separation, elongated fragments tend to return to ground-state deformation; thus, their deformation energy is converted to internal excitation energy, which leads to an increase of neutron multiplicity.

The present paper focuses on describing the charge, mass, TKE, and neutron multiplicity distributions of fission products and on comparing the calculated results with the available experimental data for fissioning thorium and uranium isotopes.

In particular, the choice of fission of Th isotopes is based on the following arguments: (1) There are reliable experimental data on the charge and TKE [13], and more recently, data on the neutron multiplicity were published in Ref. [14]. (2) The measured data on the neutron multiplicity show some interesting features, which will be discussed in the Sec. III. (3) Along the Th chain, there is a transition from a symmetric fission mode to an asymmetric one, which should be described by the fission model. Our study of the fission process is based on an improved scission-point model [15–18]. The main critical ingredient of this model is the PES, since any changes in the PES minima and their positions control all fission observables. Ultimately, the model which describes all experimentally measurable charge, mass, TKE, neutron multiplicity, and angular momentum distributions of fission fragments must provide a clear and physically sound method for calculating the PES.

II. MODEL

The most important step of the scission-point model is the calculation of the potential energy of the dinuclear system (DNS) as a function of charge Z_i , mass A_i , deformations β_i (the ratios between the major and minor semi-axes of the fragments) of the two fragments, and internuclear distance R between them [15–18]. The index i designates the light (L) or (H) heavy fragment. The scission configuration is imagined as two axially deformed and uniformly charged ellipsoids: the nascent fragments. The two nuclei are fully formed and possess all the features of isolated nuclei, e.g., binding energies, according to the separability principle, and mutually interact through the nuclear and Coulomb forces. Their orientation is frozen to a tip-to-tip configuration, which provides the minimum of interaction energy. Owing to the repulsive nature of the Coulomb interaction V^C and attractive nature of the nuclear interaction V^N , a potential pocket is formed in R coordinate with a minimum at $R = R_m$ which roughly

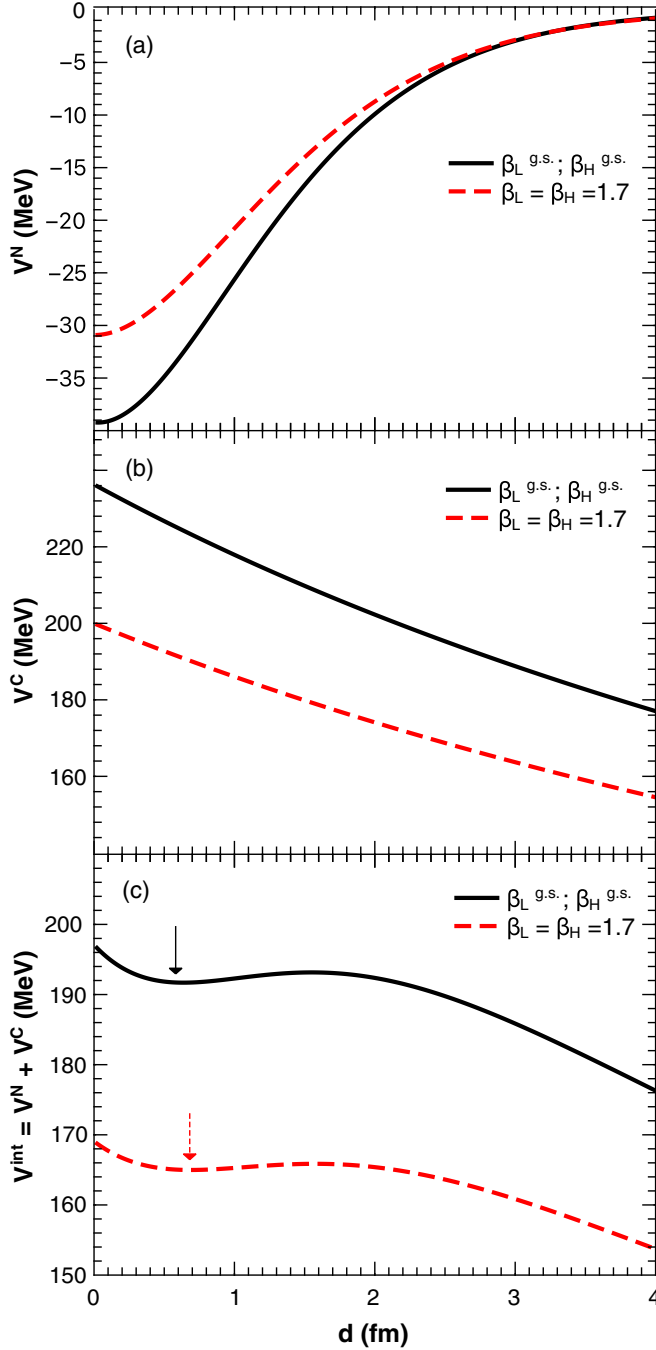


FIG. 1. The calculated nuclear V^N and Coulomb V^C interaction potentials and their sum $V^{int} = V^N + V^C$ as a function of the distance d between the tips of the fragments for the fragmentation $^{222}\text{Th} \rightarrow ^{110}\text{Ru} + ^{112}\text{Pd}$. The position of the interaction potential pocket minimum is indicated by the arrow. The deformations $\beta_{L,H}$ of the DNS nuclei are indicated.

corresponds to a separation of $d = 0.5\text{--}1$ fm between the tips of the fragments, depending on the mass $A_{L,H}$ and charge $Z_{L,H}$ numbers and deformations $\beta_{L,H}$ (see Fig. 1). The depth B_{qf} of the potential pocket insures that the DNS is in local equilibrium over all collective coordinates before the fragmentation. Because the model assumes the statistical equilibrium at

scission point, one can reduce the complexity of the problem by fixing the internuclear distance at the bottom of the potential pocket ($R = R_m$). Then, the potential energy

$$U = U_L^{LD} + \delta U_L^{\text{shell}} + U_H^{LD} + \delta U_H^{\text{shell}} + V^C + V^N \quad (1)$$

of the system is calculated as the sum of the energies of the fragments [the liquid-drop (LD) energy U_i^{LD} plus shell-correction energy $\delta U_i^{\text{shell}}$] and energy $V^{int} = V^C + V^N$ of the fragment-fragment interaction [15–18]. The interaction potential consists of the Coulomb interaction potential V^C of two uniformly charged ellipsoids and nuclear interaction potential V^N taken in the double-folding form [19,20]. The nuclear densities are taken in the two-parameter Woods-Saxon form with the diffuseness parameter $a = 0.51\text{--}0.56$ fm depending on the charge number of the nucleus. The energy of the nuclear interaction reaches values of about $-(25\text{--}40)$ MeV for the touching nuclei depending on their deformations (Fig. 1). Antisymmetrization between the nucleons belonging to different fragments is regarded by a density dependence of the nucleon-nucleon force which gives a repulsive core in the fragment-fragment interaction potential [19]. As seen in Fig. 1, for the fragmentation $^{222}\text{Th} \rightarrow ^{110}\text{Ru} + ^{112}\text{Pd}$, the interaction potential has an inner pocket and an external Coulomb barrier located at the distances d between the tips of the fragments of 0.6 fm (0.7 fm) and 1.5 fm (1.6 fm), respectively, at the ground state deformations of fragments (at $\beta_L = \beta_H = 1.7$). The absolute value of the nuclear (Coulomb) interaction at high deformations is about 9 (34) MeV less than for the deformations of the ground state.

The shell corrections are calculated with the Strutinsky method for an axially deformed nucleus [21]. The damping of the shell correction with excitation energy E_i^* is introduced as

$$\begin{aligned} \delta U_i^{\text{shell}}(A_i, Z_i, \beta_i, E_i^*) \\ = \delta U_i^{\text{shell}}(A_i, Z_i, \beta_i, E_i^* = 0) \exp[-E_i^*/E_D], \end{aligned}$$

where $E_D = 18.5$ MeV is the damping constant. The DNS excitation energy

$$E^* = E_{CN}^* + [U_{CN}(A, Z, \beta) - U(A_i, Z_i, \beta_i, R_m)] \quad (2)$$

(U_{CN} and E_{CN}^* are the binding and excitation energies of the CN, respectively) is assumed to be distributed between the fragments proportional to their masses: $E_i^* = E^* A_i / A_{CN}$. The symmetry U_i^{sym} , Coulomb U_i^C , and surface U_i^{sur} parts of LD energy U_i^{LD} are calculated as

$$\begin{aligned} U_i^{\text{sym}} &= 27.612 \frac{(N_i - Z_i)^2}{A_i} [1 + 6 \times 10^{-4} E_i^* / A_i], \\ U_i^C &= \frac{3}{5} \frac{Z_i^2 e^2}{R_{0i}} \frac{\beta_i^{1/3}}{\sqrt{\beta_i^2 - 1}} \ln \left[\beta_i + \sqrt{\beta_i^2 - 1} \right] [1 - 0.12 E_i^* / A_i], \\ U_i^{\text{sur}} &= \sigma_i S_i [1 + 0.102 E_i^* / A_i], \end{aligned} \quad (3)$$

where $R_{0i} = 1.2249 A_i^{1/3} [1 + 5.04 \times 10^{-3} E_i^* / A_i]$ fm is the radius of the equivalent spherical fragment, S_i is the area of nuclear surface, $\sigma_i = \sigma_{0i} [1 + k_i (\beta_i - \beta_i^{g.s.})^2] f(Z_i)$ is the deformation-dependent surface tension coefficient with $\sigma_{0i} = 0.9517 [1 - 1.7826 (N_i - Z_i)^2 / A_i^2]$, $f(Z_i) =$

$1 - 0.00025(Z_i - Z_r)^2$, $Z_r = Z/2 - [15.55 - 0.25(N - Z)]$, and stiffness coefficient $k_i(E_i^*) = 0.06 \exp(-E_i^*/0.7) / \{1 + \exp(-0.063[C_{vib}(Z_i, A_i) - 67])\}$. Here, $\beta_i^{g.s.}$ and $C_{vib}(Z_i, A_i)$ are the ground-state deformation and stiffness of the nucleus, respectively [22,23]. The terms in Eq. (3) depend on the isotopic composition of the nuclei (N_i, Z_i), their deformation β_i , and excitation energy E_i^* . The excitation energy dependence of the LD terms is taken in a similar way as in Ref. [24].

The relative formation and decay probability of the DNS with particular masses, charges, and deformations of the fragments is calculated within the statistical approach as follows [15–18]:

$$w(A_i, Z_i, \beta_i, E^*) = N_0 \exp \left[-\frac{U(A_i, Z_i, \beta_i, R_m) + B_{qf}(A_i, Z_i, \beta_i)}{T} \right], \quad (4)$$

where N_0 is the normalization factor. In Eq. (4), the temperature is calculated as $T = \sqrt{E^*/a}$ where $a = A/12 \text{ MeV}^{-1}$ is the level density parameter. We use a single temperature corresponding to the DNS with the lowest potential energy U , before the attenuation of the shell corrections. In order to obtain the relative yield of a particular primary fragment with the mass number A_i and atomic number Z_i , one should integrate Eq. (4) over β_L and β_H :

$$Y(Z_i, A_i) = \int d\beta_L d\beta_H w(A_i, Z_i, \beta_i, E^*). \quad (5)$$

For the calculations of mass and charge distributions, the following expressions are obtained:

$$Y(A_i) = \sum_{Z_i} \int d\beta_L d\beta_H w(A_i, Z_i, \beta_i, E^*),$$

$$Y(Z_i) = \sum_{A_i} \int d\beta_L d\beta_H w(A_i, Z_i, \beta_i, E^*). \quad (6)$$

These distributions are normalized to unity. Note that, in order to simulate the minimal experimental uncertainties, the mass yields in our work are smoothed using the Gaussian function with width $\sigma = 0.5 \text{ u}$. The charge yields are not smoothed.

The scission-point model is also suitable for describing the TKE of the fission fragments. Supposing that all nucleus-nucleus interaction energy transforms after fission into the TKE of the DNS primary fragments with (A_i, Z_i) ,

$$\text{TKE}(A_i, Z_i, \beta_i) = V^C(A_i, Z_i, \beta_i, R_b) + V^N(A_i, Z_i, \beta_i, R_b),$$

we calculate the mean value of the TKE as a function of fragment charge Z_i by averaging over the deformations of the primary fragments and summing over the mass numbers A_i :

$$\langle \text{TKE} \rangle(Z_i) = \frac{\sum_{A_i} \int d\beta_L d\beta_H \text{TKE}(A_i, Z_i, \beta_i) w(A_i, Z_i, \beta_i, E^*)}{\sum_{A_i} \int d\beta_L d\beta_H w(A_i, Z_i, \beta_i, E^*)}. \quad (7)$$

Because of the excitation energy, the primary fragment evaporates several neutrons after fission changing the mass yields. To calculate the average number of neutrons emitted by the DNS with charge numbers Z_i ($i = L, H$), the expression

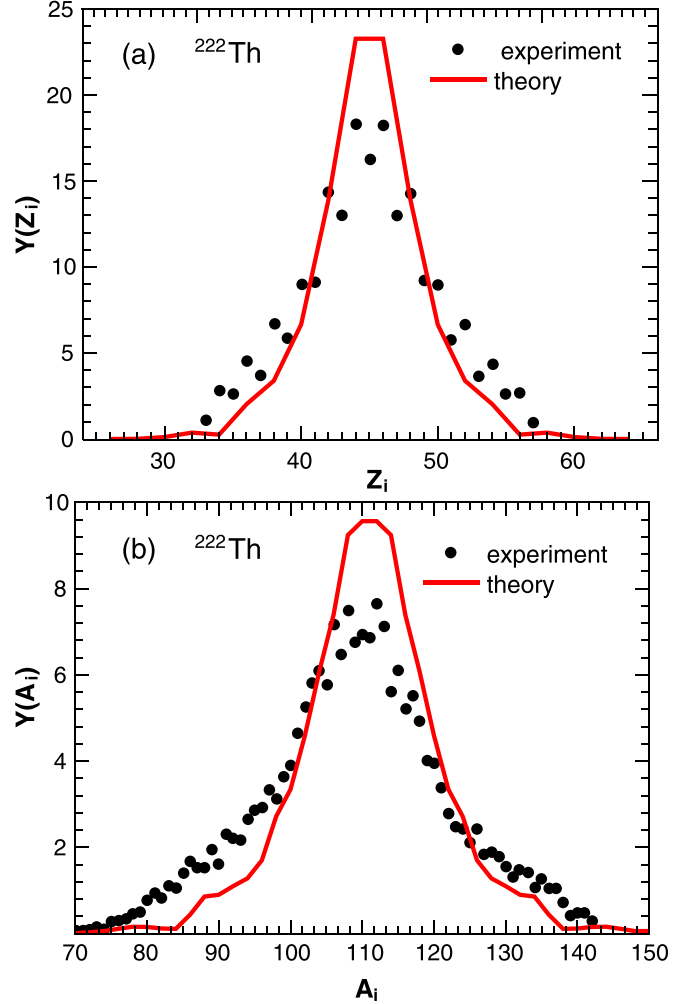


FIG. 2. The calculated (lines) and experimental (symbols) [13,14] charge (a) and mass (b) distributions of fission fragments for electromagnetic induced fission of ^{222}Th at 11 MeV excitation energy. The lines connect the calculated points for even-even fission fragments.

used is

$$\langle n \rangle(Z_i) = \frac{\sum_{A_i} \int d\beta_L d\beta_H n(A_i, Z_i, \beta_i) w(A_i, Z_i, \beta_i, E^*)}{\sum_{A_i} \int d\beta_L d\beta_H w(A_i, Z_i, \beta_i, E^*)}, \quad (8)$$

where

$$n(A_i, Z_i, \beta_i) = \sum_{i=L,H} \frac{E_i^*(A_i, Z_i, \beta_i) + E_i^{\text{def}}(A_i, Z_i, \beta_i)}{S_i^n + 2T_i}. \quad (9)$$

The values of S_i^n are the average separation energies of the first two neutrons. In order to remove the uncertainties in the calculation of the binding energies at very large deformations, in Eqs. (7) and (8) we perform the integration over deformation coordinates only around the local minima in the PES [22,25]. The term $2T_i$ accounts for the average kinetic energy carried away by a neutron. Since the fragments are deformed at scission, the relaxation of the deformations to the ground-state deformations occurs after the DNS decay and

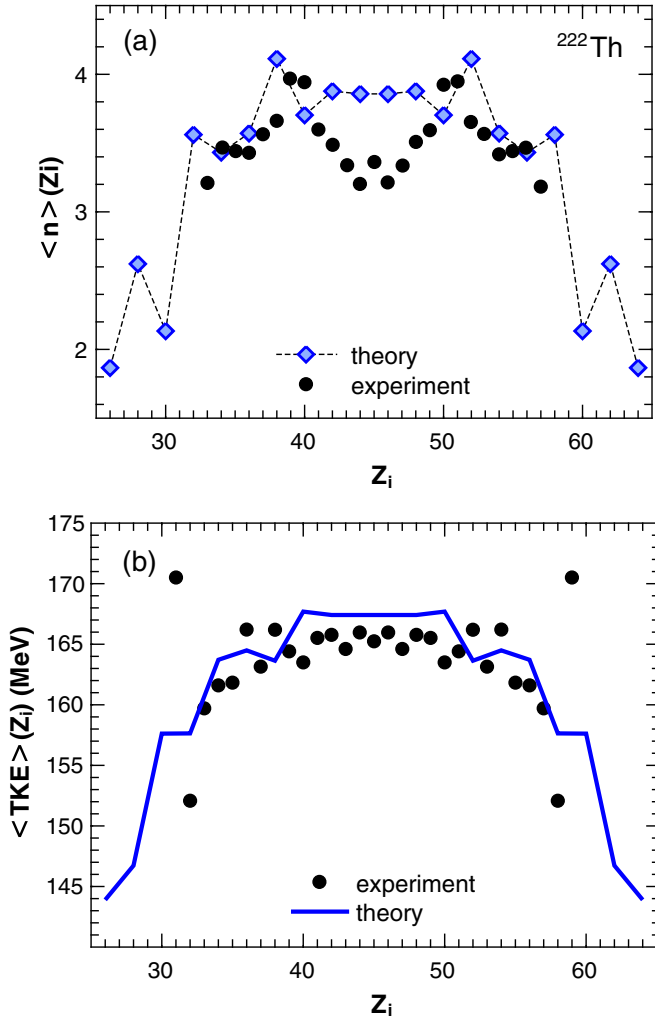


FIG. 3. The calculated (lines) and experimental (closed symbols) [13,14] neutron multiplicity (a) and TKE (b) distributions for electromagnetic induced fission of ^{222}Th at 11 MeV excitation energy.

the energies E_i^{def} of deformations are transformed into the fragment intrinsic excitation energies.

III. RESULTS AND DISCUSSIONS

In Figs. 2–7, the calculated charge, mass, TKE, and neutron multiplicity distributions of fission fragments resulting from the electromagnetic ($E_\gamma^* = 11$ MeV) induced fission of $^{222,226,230}\text{Th}$ are compared with the available experimental data [13,14,26]. The experimental (calculated) mass distributions refer to secondary (primary) fission products. Note that the calculated charge distributions differ only slightly from those in Ref. [15], although we previously used the constraint on the barrier B_{qf} (or excluded strongly deformed configurations) and other parametrization of the surface potential energy U_i^{sur} . So, the calculated results are stable with respect to reasonable variations of the model parameters.

As seen in Figs. 2–7, the mass, charge, TKE, and neutron multiplicity distributions of fission fragments are well reproduced. For the fissioning nuclei $^{222,226}\text{Th}$, the TKE distri-

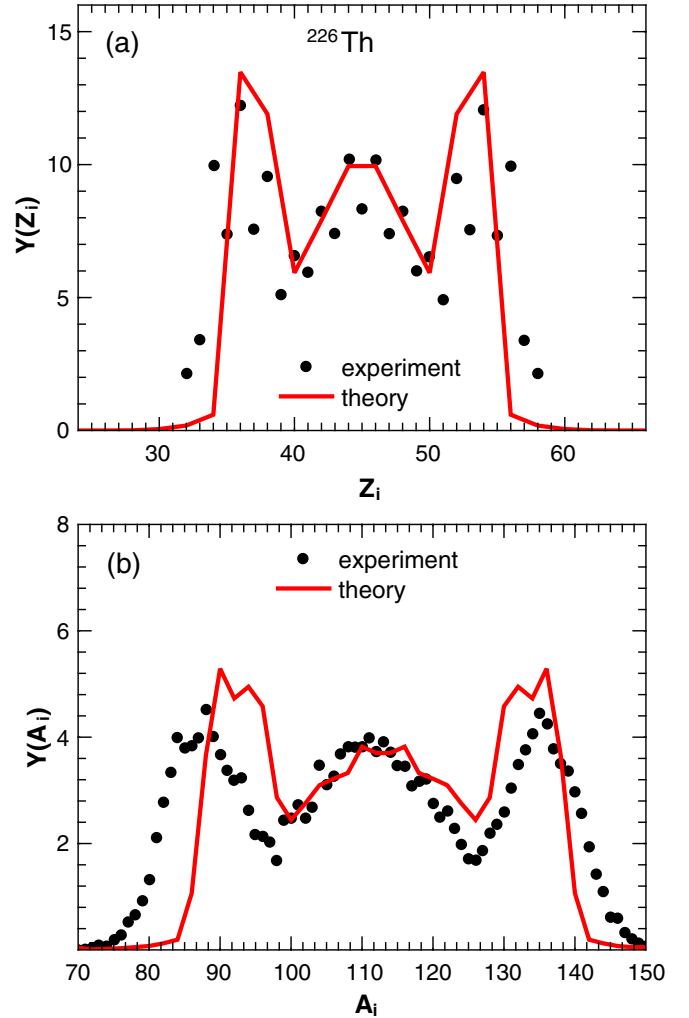


FIG. 4. The same as in Fig. 2, but for electromagnetic induced fission of ^{226}Th at 11 MeV excitation energy.

butions have completely different shapes [Figs. 3(b) and 5(b)]. In the case of ^{222}Th there is the plateau at $36 < Z_i < 54$, while in the case of ^{226}Th the TKE distribution shows asymmetric “wings” and a minimum at symmetric region around $Z = Z_{\text{CN}}/2$. The difference of these distributions can be explained by noting that for ^{226}Th the asymmetric charge and mass peaks (Fig. 4) are the result of shell effects which manifest themselves much more strongly in this nucleus than in more neutron-deficient thorium isotopes. Stronger shell effects lead to the compact scission configurations and, accordingly, to larger TKE values. On other hand, in the case of ^{222}Th , the shell corrections are not strong enough to form a significant structure in the charge, mass, and TKE distributions at the magic atomic numbers. A symmetric peak in the charge and mass distributions has its origin in the LD nature of the fissioning nucleus because the symmetric fragments have mid-closed shells. Note that for ^{230}Th the predicted TKE distribution in Fig. 7(b) is similar to that for ^{226}Th in Fig. 5(b).

In Figs. 3, 5, and 7, the calculated neutron multiplicities $\langle n \rangle(Z_i)$ as functions of the charge number of one of the fragments are compared with the experimental data [14]. For the

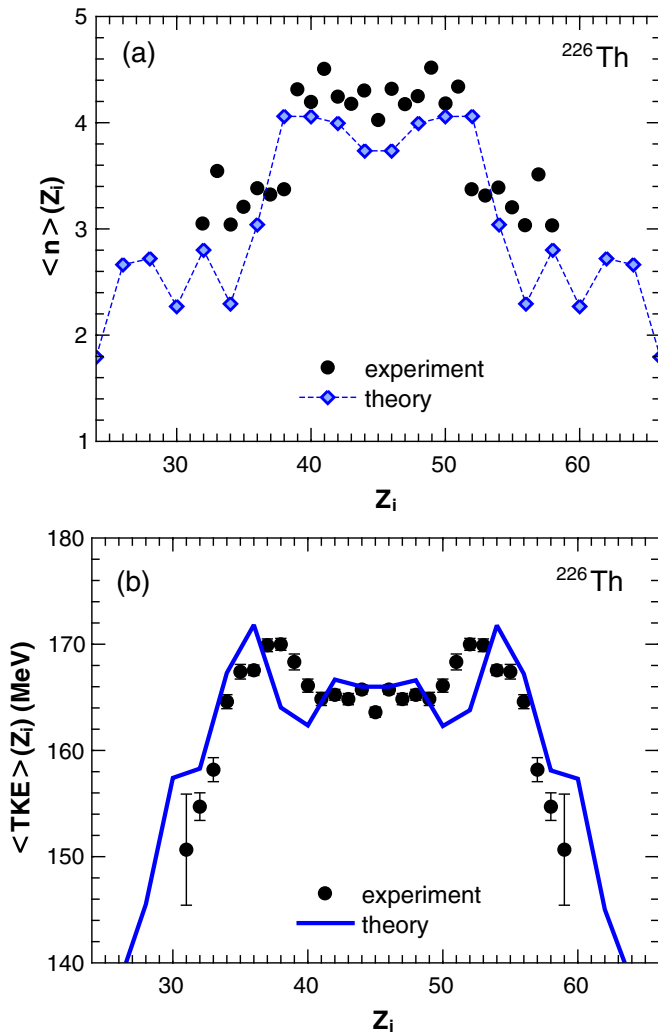


FIG. 5. The same as in Fig. 3, but for electromagnetic induced fission of ^{226}Th at 11 MeV excitation energy.

fissioning nucleus ^{222}Th , both theoretical results and experimental data show a rather constant value of $\langle n \rangle \approx 3.5$ in the region $34 < Z_i < 56$, with some fluctuations around this value. So, the neutron multiplicity is weakly dependent on the fragment charge number. The largest difference between the experimental and calculated values is ≈ 0.5 at symmetry. In the fission of ^{226}Th , the calculated neutron multiplicity distribution also agrees with the experimental data (Fig. 5). While our results slightly underestimate the experimental values, the ratio between the neutron multiplicities at symmetry and in the region $Z_i < 40$ are the same, and the increase in overall neutron multiplicity is observed as in the experiment. One notes that these distributions differ significantly from the distributions shown in Fig. 3. There is a rather strong dependence of $\langle n \rangle$ on Z_i in Fig. 5, with a pronounced increase of the neutron multiplicity in the region $40 < Z_i < 50$. In this region the shell effects are almost negligible and an almost pure LD behavior of the system causes higher deformations of fragments and low values of the potential energy U which are also seen in the TKE and charge distributions. So, the

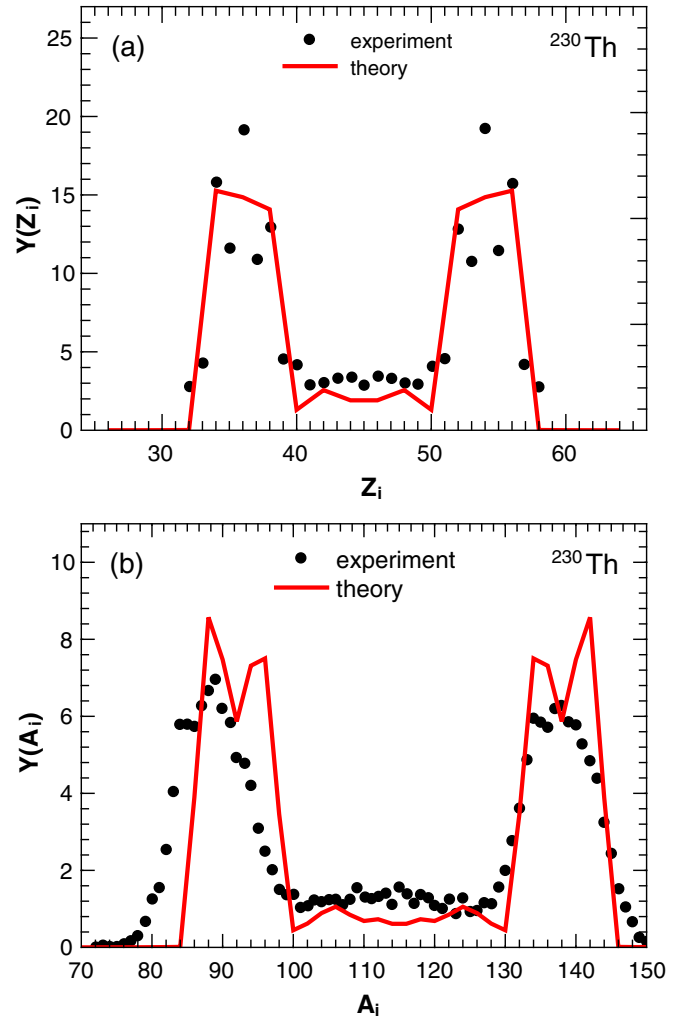


FIG. 6. The same as in Fig. 2, but for electromagnetic induced fission of ^{230}Th at 11 MeV excitation energy.

increase of the neutron multiplicity is due to an increase of both deformation and excitation energies.

In the case of ^{230}Th (Fig. 7), the shapes of the calculated and experimental neutron multiplicity distributions match each other, and the ratio between the $\langle n \rangle(Z_i)$ at symmetry and in the region $Z_i < 40$ has roughly the same value (≈ 1.7) in both experiment and in theory. However, there is a large discrepancy in the absolute values of the calculated and experimental neutron multiplicities. The measured data shows an increase of $\langle n \rangle(Z_i)$ by one unit in the region $Z_i < 40$ and almost four units at symmetry, as compared with the same distribution measured for the fissioning nucleus ^{222}Th . In our calculations, we do find an increase in the neutron multiplicity, but not as large as in the experiment. It is difficult to justify such a large increase; an increase of 3–4 units at symmetry means an increase of 25–30 MeV of the excitation energy or deformation energy. In our opinion, an increase of the excitation energy alone by 25–30 MeV is extremely unrealistic, since it would lead to symmetric charge and mass distributions. According to our estimates, the increase in the

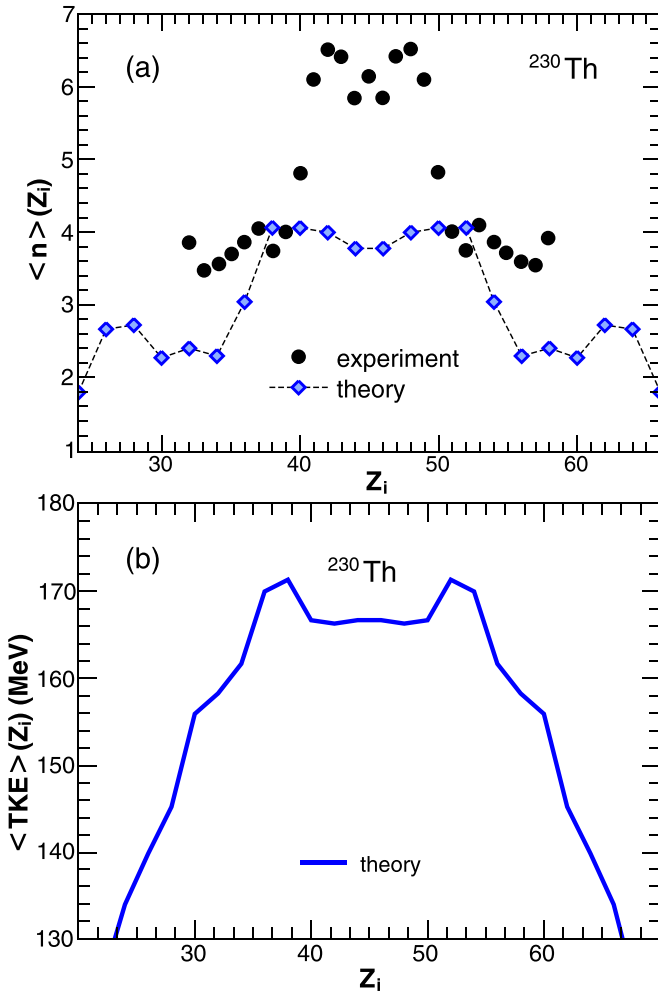


FIG. 7. The same as in Fig. 3, but for electromagnetic induced fission of ^{230}Th at 11 MeV excitation energy.

deformation energy required for the neutron multiplicity at symmetry to have a value of ≈ 7 would mean that the two fragments must have an axis ratio of more than 2.3, which is about 1.35 times larger than those in our calculations. Also, the larger $\langle n \rangle(Z_i)$ for fragments with $Z_i < 40$ are difficult to justify, since stronger shell effects lead to more compact configurations, so the deformation energy actually decreases and compensates for the increase of the excitation energy in this region. Finally, we can conclude that the experimental values of $\langle n \rangle$ for ^{230}Th are systematically overestimated.

For the electromagnetic induced fission of ^{230}U and ^{234}U at an average excitation energy $E^* = 11$ MeV (Fig. 8) the asymmetric nature of the charge and TKE distributions is fairly well reproduced. For ^{230}U , the TKE distribution at symmetry shows a rather weak dependence on Z_i , while the neutron multiplicity represents an almost constant value (≈ 4.2) in the region $40 < Z_i < 50$ with a small hump at symmetry correlating with the minima of $\langle \text{TKE} \rangle(Z_i)$ and $Y(Z_i)$. In the region $40 < Z_i < 50$, the fragments behaves like liquid drops (as for ^{230}Th), so large deformations of fragments create these features. For ^{234}U , we again predict a rather weak depen-

dence of $\langle n \rangle$ on Z_i at symmetry. Note that the values of the average neutron multiplicities at symmetry decrease with increasing mass number of uranium isotopes from 230 to 234, although for thorium isotopes we observe the opposite trend. The explanation of this behavior is as follows: It is known that neutron-deficient U isotopes provide higher charge and mass yields at symmetry than neutron-rich U isotopes, with larger excitation energy at symmetry. On the other hand, the positions of the minima in the PES for symmetric fragmentations of neutron-rich uranium nuclides are located at slightly lower deformations $\beta_{L,H}$, so the deformation energies are also slightly smaller. The combined influence of these two factors generally results in slightly lower values of $\langle n \rangle$ in ^{234}U .

IV. CONCLUSIONS

As shown, the improved scission-point model of fission is able to consistently and reliably describe several fission observables of interest for fissioning nuclei $^{222,226,230}\text{Th}$ and $^{230,234}\text{U}$ at an average excitation energy $E^* = 11$ MeV. The description of charge, mass, TKE, and neutron multiplicity distributions of fission fragments is based on the same PES. It is demonstrated that all these distributions are correlated and the transition from the asymmetric to the symmetric fission regime, which occurs along the Th isotope chain, leads to an increase of the neutron multiplicity at symmetry. For the fissioning thorium isotopes, the transition from a symmetric fission mode to an asymmetric one is also reproduced.

As found for a fissioning nucleus ^{222}Th , almost constant value of TKE at symmetry is associated with a fairly constant value of the neutron multiplicity. As the Th mass number increases, the role of shell corrections becomes dominant, and the TKE and neutron multiplicity distributions closely follow the changes occurring in the PES of the system. In the case of ^{226}Th , the asymmetric peaks in the charge distribution resulting from the shell corrections are closely related to the asymmetric humps found in the TKE distribution, while the symmetric peak in the charge yields is associated with lower TKE and higher neutron multiplicities at symmetry due to the LD behavior of the system. As the mass number of Th increases from 226 to 230, the strong shell effects impose a dominant asymmetric fission mode, which provides asymmetric maxima in charge yields. For the fissioning ^{230}Th , the TKE distribution also presents the shell effects and the calculated neutron multiplicities show a slight increase at symmetry. Note that the shape of the calculated distribution of neutron multiplicity is similar to the measured one, but we cannot explain the large experimental values, especially at symmetry. Nevertheless, the increase of the neutron multiplicity at symmetry with the transition from light to heavy thorium isotopes is, in our opinion, indisputable. The opposite trend is predicted for fissioning uranium isotopes.

ACKNOWLEDGMENTS

The authors are grateful to the support of the Romania-JINR (Dubna) Cooperation Programme. The work of H.P. was supported by a grant of the Ministry of Research, Innovation and Digitization, CNCS/CCCDI-UEFISCDI, Project

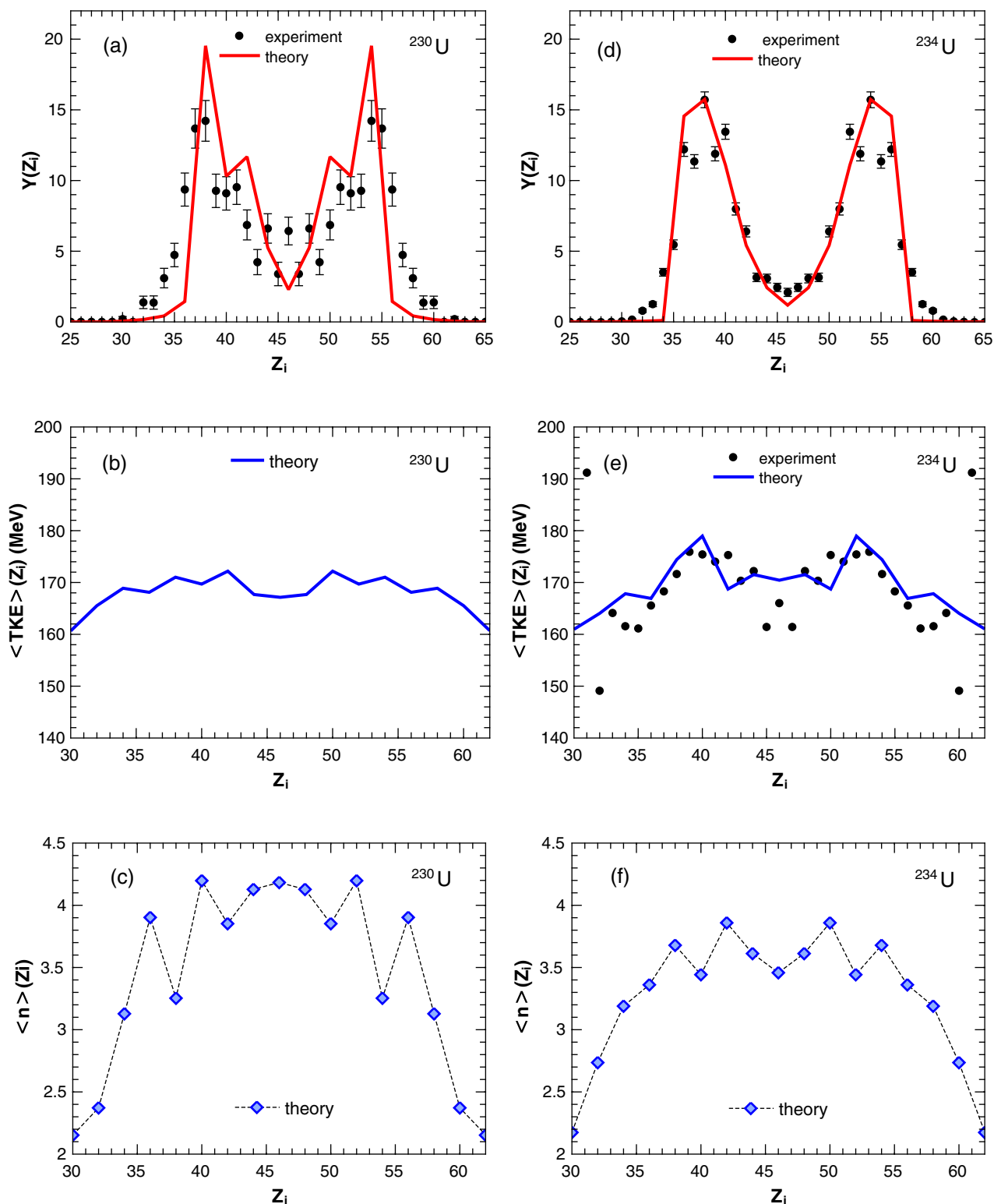


FIG. 8. The calculated (lines) and experimental (closed symbols) [13,27] charge [(a), (d)], TKE [(b), (e)], and neutron multiplicity [(c), (f)] distributions of fission fragments for electro-magnetic induced fission of $^{230,234}\text{U}$ at 11 MeV excitation energy. The lines connect the calculated points for even-even fission fragments.

No. PN-III-P1-1.1-PD-2019-0304 within PNC DI III. The work of G.G.A., N.V.A., and H.P. was supported by the

Ministry of Science and Higher Education of the Russian Federation (Contract No. 075-10-2020-117).

- [1] A. N. Andreyev, M. Huyse, and P. Van Duppen, *Rev. Mod. Phys.* **85**, 1541 (2013).
- [2] I. V. Ryzhov *et al.*, *Phys. Rev. C* **83**, 054603 (2011).
- [3] V. Simukhin, Ph.D. thesis, Uppsala University, 2010 (unpublished); I. V. Ryzhov *et al.*, *J. Korean Phys. Soc. C* **59**, 1864 (2011); V. Simukhin *et al.*, *Nucl. Data Sheets* **119**, 331 (2014).
- [4] J. King *et al.*, *Eur. Phys. J. A* **53**, 238 (2017).
- [5] R. Légouillon *et al.*, *Phys. Lett. B* **761**, 125 (2016); K. Hirose *et al.*, *Phys. Rev. Lett.* **119**, 222501 (2017).
- [6] H. Naik, T. N. Nathaniel, A. Goswami, G. N. Kim, M. W. Lee, S. V. Suryanarayana, S. Ganesan, E. A. Kim, M. H. Cho, and K. L. Ramakumar, *Phys. Rev. C* **85**, 024623 (2012); **85**, 039905(E) (2012); H. Naik *et al.*, *Nucl. Phys. A* **913**, 185 (2013); **941**, 16 (2015); **952**, 100 (2016).
- [7] A. Deppman, E. Andrade-II, V. Guimarães, G. S. Karapetyan, and N. A. Demekhina, *Phys. Rev. C* **87**, 054604 (2013); A. Deppman, E. Andrade-II, V. Guimarães, G. S. Karapetyan, A. R. Balabekyan, and N. A. Demekhina, *ibid.* **88**, 024608 (2013); A. Deppman *et al.*, *ibid.* **88**, 064609 (2013).
- [8] D. Ramos *et al.*, *Phys. Rev. C* **97**, 054612 (2018); **99**, 024615 (2019).
- [9] D. Ramos *et al.*, *Phys. Rev. Lett.* **123**, 092503 (2019).
- [10] K. Nishio *et al.*, *Phys. Lett. B* **748**, 89 (2015).
- [11] E. Prasad *et al.*, *Phys. Rev. C* **91**, 064605 (2015); *Phys. Lett. B* **811**, 135941 (2020).
- [12] I. Tsekhanovich *et al.*, *Phys. Lett. B* **790**, 583 (2019).
- [13] K.-H. Schmidt *et al.*, *Nucl. Phys. A* **665**, 221 (2000); **693**, 169 (2001).
- [14] A. Chatillon *et al.*, *Phys. Rev. Lett.* **124**, 202502 (2020).
- [15] H. Paşca, A. V. Andreev, G. G. Adamian, and N. V. Antonenko, *Phys. Lett. B* **760**, 800 (2016).
- [16] H. Paşca, A. V. Andreev, G. G. Adamian, and N. V. Antonenko, *Phys. Rev. C* **94**, 064614 (2016).
- [17] H. Paşca, A. V. Andreev, G. G. Adamian, and N. V. Antonenko, *Phys. Rev. C* **97**, 034621 (2018); *Nucl. Phys. A* **969**, 226 (2018).
- [18] H. Paşca, A. V. Andreev, G. G. Adamian, and N. V. Antonenko, *Phys. Rev. C* **101**, 064604 (2020).
- [19] G. G. Adamian *et al.*, *Int. J. Mod. Phys. E* **5**, 191 (1996).
- [20] G. G. Adamian, N. V. Antonenko, and W. Scheid, in *Clusters in Nuclei*, Vol. 2, edited by C. Beck, Lecture Notes in Physics Vol. 848 (Springer, Berlin 2012), p. 165.
- [21] J. Maruhn and W. Greiner, *Z. Phys.* **251**, 431 (1972).
- [22] A. V. Andreev, G. G. Adamian, N. V. Antonenko, S. P. Ivanova, and W. Scheid, *Eur. Phys. J. A* **22**, 51 (2004); A. V. Andreev, G. G. Adamian, N. V. Antonenko, and S. P. Ivanova, *ibid.* **26**, 327 (2005); A. V. Andreev, G. G. Adamian, N. V. Antonenko, S. P. Ivanova, S. N. Kuklin, and W. Scheid, *ibid.* **30**, 579 (2006).
- [23] A. V. Andreev, G. G. Adamian, and N. V. Antonenko, *Phys. Rev. C* **86**, 044315 (2012); A. V. Andreev, G. G. Adamian, N. V. Antonenko, and A. N. Andreyev, *ibid.* **88**, 047604 (2013).
- [24] G. Sauer, H. Chandra, and U. Mosel, *Nucl. Phys. A* **264**, 221 (1976).
- [25] A. I. Svirikhin *et al.*, *Eur. Phys. J. A* **48**, 121 (2012).
- [26] A. Chatillon *et al.*, *Phys. Rev. C* **99**, 054628 (2019).
- [27] M. Asghar, F. Caitucolli, B. Leroux, P. Perrin, and G. Barreau, *Nucl. Phys. A* **368**, 319 (1981).